Fermi National Accelerator Laboratory

FERMILAB-Pub-95/317-E

CDF

Measurement of the Mass of the B_s^0 Meson

F. Abe et al.

The CDF Collaboration

Fermi National Accelerator Laboratory
P.O. Box 500, Batavia, Illinois 60510

October 1995

Submitted to *Physical Review D*

Operated by Universities Research Association Inc. under Contract No. DE-AC02-76CHO3000 with the United States Department of Energy

Disclaimer

FERMILAB-PUB-95/317-E

Measurement of the Mass of the B_s^0 Meson

F. Abe,[13] M. G. Albrow,[7] S. R. Amendolia,[23] D. Amidei,[16] J. Antos,[28] C. Anway-Wiese,[4] G. Apollinari,[26] H. Areti,[7] M. Atac,[7] P. Auchincloss,[25] F. Azfar,[21] P. Azzi,[20] N. Bacchetta,[20] W. Badgett,[16] M. W. Bailey,[18] J. Bao,[35] P. de Barbaro,[25] A. Barbaro-Galtieri,[14] V. E. Barnes,[24] B. A. Barnett,[12] P. Bartalini,[23] G. Bauer,[15] T. Baumann,[9] F. Bedeschi,[23] S. Behrends,[3] S. Belforte,[23] G. Bellettini,[23] J. Bellinger,[34] D. Benjamin,[31] J. Benlloch,[15] J. Bensinger,[3] D. Benton,[21] A. Beretvas,[7] J. P. Berge,[7] S. Bertolucci,[8] A. Bhatti,[26] K. Biery,[11] M. Binkley,[7] F. Bird,[29] D. Bisello,[20] R. E. Blair,[1] C. Blocker,[3] A. Bodek,[25] W. Bokhari,[15] V. Bolognesi,[23] D. Bortoletto,[24] C. Boswell,[12] T. Boulos,[14] G. Brandenburg,[9] C. Bromberg,[17] E. Buckley-Geer,[7] H. S. Budd,[25] K. Burkett,[16] G. Busetto,[20] A. Byon-Wagner,[7] K. L. Byrum,[1] J. Cammerata,[12] C. Campagnari,[7] M. Campbell,[16] A. Caner,[7] W. Carithers,[14] D. Carlsmith,[34] A. Castro,[20] Y. Cen,[21] F. Cervelli,[23] H. Y. Chao,[28] J. Chapman,[16] M.-T. Cheng,[28] G. Chiarelli,[23] T. Chikamatsu,[32] C. N. Chiou,[28] L. Christofek,[10] S. Cihangir,[7] A. G. Clark,[23] M. Cobal,[23] M. Contreras,[5] J. Conway,[27] J. Cooper,[7] M. Cordelli,[8] C. Couyoumtzelis,[23] D. Crane,[1] J. D. Cunningham,[3] T. Daniels,[15] F. DeJongh,[7] S. Delchamps,[7] S. Dell'Agnello,[23] M. Dell'Orso,[23] L. Demortier,[26] B. Denby,[23] M. Deninno,[2] P. F. Derwent,[16] T. Devlin,[27] M. Dickson,[25] J. R. Dittmann,[6] S. Donati,[23] R. B. Drucker,[14] A. Dunn,[16] K. Einsweiler,[14] J. E. Elias,[7] R. Ely,[14] E. Engels, Jr.,[22] S. Eno,[5] D. Errede,[10] S. Errede,[10] Q. Fan,[25] B. Farhat,[15] I. Fiori,[2] B. Flaugher,[7] G. W. Foster,[7] M. Franklin,[9] M. Frautschi,[18] J. Freeman,[7] J. Friedman,[15] H. Frisch,[5] A. Fry,[29] T. A. Fuess,[1] Y. Fukui,[13] S. Funaki,[32] G. Gagliardi,[23] S. Galeotti,[23] M. Gallinaro,[20] A. F. Garfinkel,[24] S. Geer,[7] D. W. Gerdes,[16] P. Giannetti,[23] N. Giokaris,[26] P. Giromini,[8] L. Gladney,[21] D. Glenzinski,[12] M. Gold,[18] J. Gonzalez,[21] A. Gordon,[9] A. T. Goshaw,[6] K. Goulianos,[26] H. Grassmann,[6] A. Grewal,[21] L. Groer,[27] C. Grosso-Pilcher,[5] C. Haber,[14] S. R. Hahn,[7] R. Hamilton,[9] R. Handler,[34] R. M. Hans,[35] K. Hara,[32] B. Harral,[21] R. M. Harris,[7] S. A. Hauger,[6] J. Hauser,[4] C. Hawk,[27] J. Heinrich,[21] D. Cronin-Hennessy,[6] R. Hollebeek,[21] L. Holloway,[10] A. Hölscher,[11] S. Hong,[16] G. Houk,[21] P. Hu,[22] B. T. Huffman,[22] R. Hughes,[25] P. Hurst,[9] J. Huston,[17] J. Huth,[9] J. Hylen,[7] M. Incagli,[23] J. Incandela,[7] H. Iso,[32] H. Jensen,[7] C. P. Jessop,[9] U. Joshi,[7] R. W. Kadel,[14] E. Kajfasz,[7a] T. Kamon,[30] T. Kaneko,[32] D. A. Kardelis,[10] H. Kasha,[35] Y. Kato,[19] L. Keeble,[8] R. D. Kennedy,[27] R. Kephart,[7] P. Kesten,[14] D. Kestenbaum,[9] R. M. Keup,[10] H. Keutelian,[7] F. Keyvan,[4] D. H. Kim,[7] H. S. Kim,[11] S. B. Kim,[16] S. H. Kim,[32] Y. K. Kim,[14] L. Kirsch,[3] P. Koehn,[25] K. Kondo,[32] J. Konigsberg,[9] S. Kopp,[5] K. Kordas,[11] W. Koska,[7] E. Kovacs,[7a] W. Kowald,[6] M. Krasberg,[16] J. Kroll,[7] M. Kruse,[24] S. E. Kuhlmann,[1] E. Kuns,[27] A. T. Laasanen,[24] N. Labanca,[23] S. Lammel,[4] J. I. Lamoureux,[3] T. LeCompte,[10] S. Leone,[23] J. D. Lewis,[7] P. Limon,[7]

[0]Submitted to Physical Review **D** September 27, 1995

M. Lindgren,[4] T. M. Liss,[10] N. Lockyer,[21] C. Loomis,[27] O. Long,[21] M. Loreti,[20] E. H. Low,[21] J. Lu,[30] D. Lucchesi,[23] C. B. Luchini,[10] P. Lukens,[7] J. Lys,[14] P. Maas,[34] K. Maeshima,[7] A. Maghakian,[26] P. Maksimovic,[15] M. Mangano,[23] J. Mansour,[17] M. Mariotti,[20] J. P. Marriner,[7] A. Martin,[10] J. A. J. Matthews,[18] R. Mattingly,[15] P. McIntyre,[30] P. Melese,[26] A. Menzione,[23] E. Meschi,[23] G. Michail,[9] S. Mikamo,[13] M. Miller,[5] R. Miller,[17] T. Mimashi,[32] S. Miscetti,[8] M. Mishina,[13] H. Mitsushio,[32] S. Miyashita,[32] Y. Morita,[23] S. Moulding,[26] J. Mueller,[27] A. Mukherjee,[7] T. Muller,[4] P. Musgrave,[11] L. F. Nakae,[29] I. Nakano,[32] C. Nelson,[7] D. Neuberger,[4] C. Newman-Holmes,[7] L. Nodulman,[1] S. Ogawa,[32] S. H. Oh,[6] K. E. Ohl,[35] R. Oishi,[32] T. Okusawa,[19] C. Pagliarone,[23] R. Paoletti,[23] V. Papadimitriou,[31] S. P. Pappas,[35] S. Park,[7] J. Patrick,[7] G. Pauletta,[23] M. Paulini,[14] L. Pescara,[20] M. D. Peters,[14] T. J. Phillips,[6] G. Piacentino,[2] M. Pillai,[25] R. Plunkett,[7] L. Pondrom,[34] N. Produit,[14] J. Proudfoot,[1] F. Ptohos,[9] G. Punzi,[23] K. Ragan,[11] F. Rimondi,[2] L. Ristori,[23] M. Roach-Bellino,[33] W. J. Robertson,[6] T. Rodrigo,[7] J. Romano,[5] L. Rosenson,[15] W. K. Sakumoto,[25] D. Saltzberg,[5] A. Sansoni,[8] V. Scarpine,[30] A. Schindler,[14] P. Schlabach,[9] E. E. Schmidt,[7] M. P. Schmidt,[35] O. Schneider,[14] G. F. Sciacca,[23] A. Scribano,[23] S. Segler,[7] S. Seidel,[18] Y. Seiya,[32] G. Sganos,[11] A. Sgolacchia,[2] M. Shapiro,[14] N. M. Shaw,[24] Q. Shen,[24] P. F. Shepard,[22] M. Shimojima,[32] M. Shochet,[5] J. Siegrist,[29] A. Sill,[31] P. Sinervo,[11] P. Singh,[22] J. Skarha,[12] K. Sliwa,[33] D. A. Smith,[23] F. D. Snider,[12] L. Song,[7] T. Song,[16] J. Spalding,[7] L. Spiegel,[7] P. Sphicas,[15] L. Stanco,[20] J. Steele,[34] A. Stefanini,[23] K. Strahl,[11] J. Strait,[7] D. Stuart,[7] G. Sullivan,[5] K. Sumorok,[15] R. L. Swartz, Jr.,[10] T. Takahashi,[19] K. Takikawa,[32] F. Tartarelli,[23] W. Taylor,[11] P. K. Teng,[28] Y. Teramoto,[19] S. Tether,[15] D. Theriot,[7] J. Thomas,[29] T. L. Thomas,[18] R. Thun,[16] M. Timko,[33] P. Tipton,[25] A. Titov,[26] S. Tkaczyk,[7] K. Tollefson,[25] A. Tollestrup,[7] J. Tonnison,[24] J. F. de Troconiz,[9] J. Tseng,[12] M. Turcotte,[29] N. Turini,[23] N. Uemura,[32] F. Ukegawa,[21] G. Unal,[21] S. C. van den Brink,[22] S. Vejcik, III,[16] R. Vidal,[7] M. Vondracek,[10] D. Vucinic,[15] R. G. Wagner,[1] R. L. Wagner,[7] N. Wainer,[7] R. C. Walker,[25] C. Wang,[6] C. H. Wang,[28] G. Wang,[23] J. Wang,[5] M. J. Wang,[28] Q. F. Wang,[26] A. Warburton,[11] G. Watts,[25] T. Watts,[27] R. Webb,[30] C. Wei,[6] C. Wendt,[34] H. Wenzel,[14] W. C. Wester, III,[7] T. Westhusing,[10] A. B. Wicklund,[1] E. Wicklund,[7] R. Wilkinson,[21] H. H. Williams,[21] P. Wilson,[5] B. L. Winer,[25] J. Wolinski,[30] D. Y. Wu,[16] X. Wu,[23] J. Wyss,[20] A. Yagil,[7] W. Yao,[14] K. Yasuoka,[32] Y. Ye,[11] G. P. Yeh,[7] P. Yeh,[28] M. Yin,[6] J. Yoh,[7] C. Yosef,[17] T. Yoshida,[19] D. Yovanovitch,[7] I. Yu,[35] J. C. Yun,[7] A. Zanetti,[23] F. Zetti,[23] L. Zhang,[34] S. Zhang,[16] W. Zhang,[21] and S. Zucchelli[2]

(CDF Collaboration)

[1] *Argonne National Laboratory, Argonne, Illinois 60439*

[2] *Istituto Nazionale di Fisica Nucleare, University of Bologna, I-40126 Bologna, Italy*

[3] *Brandeis University, Waltham, Massachusetts 02254*

[4] *University of California at Los Angeles, Los Angeles, California 90024*

[5] *University of Chicago, Chicago, Illinois 60637*

[6] Duke University, Durham, North Carolina 27708
[7] Fermi National Accelerator Laboratory, Batavia, Illinois 60510
[8] Laboratori Nazionali di Frascati, Istituto Nazionale di Fisica Nucleare, I-00044 Frascati, Italy
[9] Harvard University, Cambridge, Massachusetts 02138
[10] University of Illinois, Urbana, Illinois 61801
[11] Institute of Particle Physics, McGill University, Montreal H3A 2T8, and University of Toronto, Toronto M5S 1A7, Canada
[12] The Johns Hopkins University, Baltimore, Maryland 21218
[13] National Laboratory for High Energy Physics (KEK), Tsukuba, Ibaraki 305, Japan
[14] Lawrence Berkeley Laboratory, Berkeley, California 94720
[15] Massachusetts Institute of Technology, Cambridge, Massachusetts 02139
[16] University of Michigan, Ann Arbor, Michigan 48109
[17] Michigan State University, East Lansing, Michigan 48824
[18] University of New Mexico, Albuquerque, New Mexico 87131
[19] Osaka City University, Osaka 588, Japan
[20] Universita di Padova, Istituto Nazionale di Fisica Nucleare, Sezione di Padova, I-35131 Padova, Italy
[21] University of Pennsylvania, Philadelphia, Pennsylvania 19104
[22] University of Pittsburgh, Pittsburgh, Pennsylvania 15260
[23] Istituto Nazionale di Fisica Nucleare, University and Scuola Normale Superiore of Pisa, I-56100 Pisa, Italy
[24] Purdue University, West Lafayette, Indiana 47907
[25] University of Rochester, Rochester, New York 14627
[26] Rockefeller University, New York, New York 10021
[27] Rutgers University, Piscataway, New Jersey 08854
[28] Academia Sinica, Taiwan 11529, Republic of China
[29] Superconducting Super Collider Laboratory, Dallas, Texas 75237
[30] Texas A&M University, College Station, Texas 77843
[31] Texas Tech University, Lubbock, Texas 79409
[32] University of Tsukuba, Tsukuba, Ibaraki 305, Japan
[33] Tufts University, Medford, Massachusetts 02155
[34] University of Wisconsin, Madison, Wisconsin 53706
[35] Yale University, New Haven, Connecticut 06511

Abstract

We measure the mass of the B_s^0 meson by reconstructing the decay chain $B_s^0 \to J/\psi\phi$, $J/\psi \to \mu^+\mu^-$, and $\phi \to K^+K^-$. The data are obtained from 19.3 pb^{-1} of integrated luminosity of $\overline{p}p$ collisions at $\sqrt{s} = 1.8$ TeV using the Collider Detector at Fermilab (CDF). A sample of 80,000 inclusive $J/\psi \to \mu^+\mu^-$ events is used to study systematic biases in track reconstruction and to calibrate the momentum scale. We reconstruct the kinematically similar decays $B^+ \to J/\psi K^+$ and $B^0 \to J/\psi K^{*0}$ to study the mass measurement technique used for the B_s^0 meson. Based on the observation of 32 ± 6 candidates, the mass of the B_s^0 meson is measured to be $5369.9 \pm 2.3 \pm 1.3$ MeV/c^2 and the mass difference between B_s^0 and the average mass of B^+ and B^0 is determined to be $89.7 \pm 2.7 \pm 1.2$ MeV/c^2.

PACS Numbers: 13.25.+m, 14.40.Jz

1 Introduction

The Fermilab Tevatron and the Collider Detector at Fermilab (CDF) provide a rich environment for studies of B hadrons [1] because of the large (50 μb [2, 3]) cross section for $b\bar{b}$ production. Fully reconstructed B hadrons are observed in $B \to J/\psi X$ decay modes ($X = K$, K^{*0}, ϕ) where the $J/\psi \to \mu^+\mu^-$ decay provides a convenient trigger. From the full reconstruction the of $B_s^0 \to J/\psi\phi$ decay, the mass of the B_s^0 meson is measured.

Non-relativistic Quark Models predict a B_s^0 mass in the range of 5345 to 5388 MeV/c^2 [4]. The B_s^0 mass is sensitive to constituent quark masses, the QCD potential, the wave function at the origin, and relativistic corrections. Recent lattice QCD calculations [5] predict the mass splitting of the B_s^0 and B^+ states to be $87 \pm 12\ ^{+7}_{-9}$ MeV/c^2. Agreement with experimental measurements would provide support for using the multistate smearing technique employed in these calculations.

The previous world average mass of the B_s^0 meson is 5375 ± 6 MeV/c^2 [6] which includes the results obtained by by experiments performed at LEP [7] and the value obtained by CDF in Ref. [8]. This paper updates that CDF result using the entire 1992-1993 data sample (19.3 pb^{-1}) with improved track reconstruction.

2 Detector

The CDF detector has been described in detail elsewhere [9, 10]. It is shown schematically in Fig. 1. A silicon vertex detector (SVX) [11] consisting of four layers of silicon strip detectors located between radii of 2.9 and 7.9 cm and extending $\pm$ 25 cm in z from the center of the detector provides spatial measurements for charged tracks with a resolution of 13 μm in the r-ϕ plane [12]. The geometric acceptance for the SVX is $\sim$ 60% as the interactions are distributed along the beam axis with a RMS width of $\sim$ 30 cm. Surrounding the SVX is a time projection chamber (VTX) which provides tracking measurements in the r-z plane. The VTX is used in this analysis to provide the event vertex position in z. Momenta of charged particles are measured in three dimensions by the central tracking chamber (CTC), an 84-layer drift chamber which covers the pseudorapidity interval $|\eta| < 1.1$ where $\eta = -\ln[\tan(\theta/2)]$. The 84 layers are divided into 9 alternating superlayers of 12-wire axial and 6-wire 3° stereo sense wires. The SVX, VTX, and CTC are located in an axial magnetic field with an average strength of 14.1 kG. Electromagnetic and hadronic calorimeters are located outside the tracking volume. Muons are identified using three different subsystems each consisting of four layers of drift chambers. The central muon chambers (CMU), located behind $\sim$ 5 absorption lengths of calorimeter, cover 85% of ϕ in the range $|\eta| < 0.6$. Gaps in ϕ coverage are filled in part by the central upgrade muon chambers (CMP) with total coverage in ϕ of 85% and $|\eta| < 0.6$. These chambers are located behind a total of $\sim$ 8 absorption lengths. Finally, central extension muon chambers (CMX) provide 67% coverage in ϕ for the region $0.6 < |\eta| < 1.0$ behind $\sim$ 6 absorption lengths. The muon system provides the means for identifying and triggering on events containing $J/\psi \to \mu^+\mu^-$ decays. The large tracking volume with

the CTC and SVX and strong magnetic field provide excellent momentum resolution ($\delta P_T/P_T \sim 0.001 \times P_T$ (GeV/c)).

3 $J/\psi \rightarrow \mu^+\mu^-$ Sample

3.1 Trigger

Dimuon events are collected using a three-level trigger. The Level 1 trigger requires two muon chamber track segments consistent with a P_T larger than 3.3 GeV/c. The trigger efficiency rises from 50% for muons with P_T of 1.6 GeV/c to 90% for muons with P_T of 3.1 GeV/c with a plateau of 94%. For most of the run, one of the muon segments was required to be in the CMU. At Level 2, at least one of the two muon track segments is required to match a track in the CTC found by a hardware fast track processor (CFT). A P_T requirement at level 2 is 50% efficient at 2.65 GeV/c and 90% efficient at 3.1 GeV/c with a plateau of 93%. If a CMX muon is involved, it is required to have a matched CFT track. In addition, hadronic energy deposition in the calorimeter tower towards which the muon track points is required to be larger than 0.5 GeV as expected for a minimum ionizing particle. In Level 3, software event reconstruction is performed. Dimuon J/ψ candidates are selected by imposing the requirement that two oppositely charged muons ($P_T > 1.4$ GeV/c) have extrapolated CTC tracks matching muon chamber track segments to within 4 σ (based on multiple scattering calculations). In addition, the invariant mass of the dimuon is required to be between 2.8 and 3.4 GeV/c^2.

3.2 Offline Reconstruction

Dimuon events which pass all three levels of trigger requirements are processed offline using improved calibration constants and track reconstruction algorithms. In the presence of a uniform axial magnetic field, a charged particle will travel in a helical trajectory that can be described using five track parameters (cylindrical coordinates): curvature, **C** (inverse diameter of the circle obtained by projecting the helix in the r-ϕ plane signed by the particle's charge); cotθ; impact parameter, d_0; ϕ_0; and z_0; where the subscript, 0 indicates that the parameter is with respect to the point of closest approach to the nominal beam axis. The transverse momentum of a track is inversely proportional to the curvature and proportional to the axial magnetic field:

$$P_T(\mathrm{GeV}/c) = 0.5 \times 10^{-14} c(\mathrm{cm/s}) \frac{\mathrm{B(kG)}}{\mathbf{C}(\mathrm{cm}^{-1})} = \frac{\kappa}{\mathbf{C}} \qquad (1)$$

where c is the speed of light and κ is defined by this equation. Track candidates are found in the CTC using road-based pattern recognition algorithms. Track parameters of a given track are determined by fitting tracking chamber hits to a trajectory of a helix which is perturbed because of small non-uniformities in the magnetic field [13]. If a well-matched pattern of SVX hits is found when extrapolating the CTC track into the SVX volume, those hits are included in the fit, generally improving the resolution

of $\mathbf{C}$, d_0, and ϕ_0. In addition to determining the five helical track parameters, the track fitting procedure also determines a covariance matrix which expresses measurement uncertainties of the five track parameters and their correlations (including effects such as multiple scattering). We find that we must multiply all of the elements of the covariance matrix by a factor of 1.8 so that the CTC-SVX matching uncertainty agrees with the measured resolution. The underestimation of the covariance matrix is due in part to the fact that multiple scattering within the volume of the CTC (gas and wires) is not accounted for in the track fitting procedure.

3.3 Final J/ψ Selection

For J/ψ reconstruction, the two muon tracks are constrained to come from a common vertex. The effect of this constraint is to improve the mass resolution as determined by a single Gaussian fit from 22 to 17 MeV/c^2. To select $J/\psi \to \mu^+\mu^-$ candidates, a minimal set of selection criteria are used. Matching between the extrapolated track and the hits in the muon chambers are required to be within 3 σ in r-ϕ and 3.5 σ in z for the CMU chamber where σ represents the expected uncertainty in extrapolation due to multiple scattering. These requirements remove approximately 10% of the background while preserving $> 99\%$ of the signal. Figure 2 shows the CDF dimuon mass spectrum. For B hadron reconstruction, J/ψ candidates are those dimuons with a vertex constrained dimuon mass within 100 MeV/c^2 of the world average J/ψ mass of 3096.93 MeV/c^2 [6].

4 Track Corrections and Momentum Scale

Compared with the results of Ref. [8], improvements in the offline reconstruction are made with the alignment of the SVX to the CTC, internal CTC calibration, and in using measured non-uniformities in the solenoidal magnetic field. We first describe calibrations and corrections applied to the nominal CTC and SVX track reconstruction. High statistics studies with $J/\psi \to \mu^+\mu^-$ decays and with high energy electrons, where energy and momentum are measured independently, are used to provide corrections to the reconstructed tracks. These improvements affect the overall mass resolution and also remove several systematic effects. After these corrections have been made, we use the reconstructed J/ψ mass to determine the momentum scale. In the next section, we discuss B meson reconstruction at CDF.

4.1 CTC Calibration and False Curvature

The CTC is aligned and calibrated in several steps in order to determine the relationship between drift time and distance to a sense wire. Electronic pulsing calibrations are used to determine the relative time pedestal for each sense wire. Additional corrections from the data are applied if non-uniformities are found as a function of time. The relative position of each of the 84 CTC layers is calibrated by requiring the ratio of energy to momentum, E/P, of high-P_T electrons, to be charge independent.

The alignment procedure is iterative. The $J/\psi \to \mu^+\mu^-$ sample can be used to illustrate the effect of these calibrations. Before the final alignment, a false curvature systematic effect ($\mathbf{C}_{fitted} = \mathbf{C}_{true} + \delta$) was present as can be seen in studying the reconstructed J/ψ mass as a function of the difference in curvature between the positive and negative muon (Fig. 3). After final alignment, there is no statistically significant remaining false curvature. It should be noted that for the case of a charge symmetric decay such as $B_s^0 \to J/\psi\phi$ with $J/\psi \to \mu^+\mu^-$ and $\phi \to K^+K^-$ (equal numbers of positively and negatively charged tracks with the same momentum spectrum in the final state), a false curvature systematic effect would worsen the resolution but result in no systematic shift in the average mass.

Electron candidates are measured both by the calorimeter and tracking chamber. The ratio of E/P for these candidates should not show an asymmetry between positive and negative electrons over the detector geometry. In studies used by CDF to measure the W boson mass [14], systematic mismeasurements are observed where the fitted curvature is a function of ϕ and $\cot\theta$. The following correction was derived and is used in this analysis:

$$\delta(\mathbf{C}) = \kappa \times [-0.00025 \times \sin(\phi - \Phi) - 0.00035 \times (\cot\theta + z_{vertex}/187)]\ (cm^{-1}) \quad (2)$$

where Φ equals 3.6 radians and z_{vertex} is measured in cm. As these corrections average to zero over the detector geometry and there is no statistically significant asymmetry in B decays over the detector geometry, no systematic uncertainty will be assigned for the B meson mass determination.

4.2 Corrections for Energy Loss

Corrections of track parameters due to dE/dx losses are based on extrapolating particles through a model of the known detector material from the particle's origin through the inner wall of the CTC (before the track is measured). Photons which convert into electron-positron pairs are reconstructed as a function of radius. The normalization of the material is obtained by measuring the conversion rate in the inner CTC support cylinder where the amount and composition of material is precisely known. The result is that the amount of material before the gas volume of the CTC corresponds to $8.1 \pm 0.4\%$ radiation lengths. For $J/\psi \to \mu^+\mu^-$ decays, without correcting for the energy loss, the mass would be measured low by $3.6 \times (1 + \delta D)$ MeV/c^2 where $\delta D = (^{+0.15}_{-0.24})$. δD expresses the uncertainty in the dE/dx correction which is dominated by the incomplete knowledge of the composition of materials between the beam and the CTC. The uncertainty in the dE/dx correction dominates the momentum scale uncertainty and contributes to a systematic uncertainty in the B meson mass determination. We also apply an additive correction to the dimuon mass of 0.8 ± 0.2 MeV/c^2 to account for the effect of internal bremsstrahlung on the mass fit. The correction and its uncertainty are based on Monte Carlo studies of the process.

4.3 $\Delta \cot\theta$ Systematic Effect

The longitudinal momentum, P_z, is expressed in terms of P_T and the $\cot\theta$ track parameter.

$$P_z = P_T \cot\theta \tag{3}$$

Figure 4 shows the fitted J/ψ mass in bins of the difference in $\cot\theta$ for the two muons. A large systematic effect is seen (top). A correction is applied to scale $\cot\theta$ by a factor 0.9985 which lessens the dependence (bottom). The root cause of this systematic effect is not completely understood. In evaluating systematic uncertainties, the correction 0.9985 will be modified by $\pm$ 0.0008 (chosen as half the total correction) to estimate the systematic effect on measuring the masses of the B mesons. In Fig. 4, a slight slope as a function of $\Delta \cot\theta$ is observed after the correction is applied. A possible physical interpretation is a small twist between the two CTC endplates. This slope is within the bounds of the variation of the $\cot\theta$ scale factor used for evaluating systematic uncertainties shown by the dotted lines in Fig. 4.

4.4 Additional Studies for Systematic Tracking Effects

A number of additional studies using the high statistics J/ψ sample have been performed to examine possible systematic tracking effects. The reconstructed J/ψ mass as a function of time throughout the data taking period shows some systematic structure of order 0.4 MeV/c^2. These fluctuations are larger than could be explained by monitored small magnetic field fluctuations. No systematic uncertainty is assigned because both the J/ψ mass and B meson mass reconstruction are averaged over the entire data taking period. Another check has been to look for a systematic effect in the J/ψ mass when a muon passes through the extreme edges of the tracking volume where residual magnetic field non-uniformities would be expected to be most prevalent. There is no observed statistically significant systematic effect. A systematic effect has been found due to a small mis-alignment of the axial magnetic field and detector axis. This effect causes no shift since it is averaged over ϕ. Other checks which show no systematic effects include studying the mass difference between J/ψ reconstructed with and without the vertex constraint and studying the mass difference between using and not using SVX information.

The reconstructed J/ψ mass has been examined as a function of the inverse ${P_T}^2$ averaged for the two muons (a possible higher order systematic effect in **C**). There is no statistical evidence of a systematic effect over the P_T range probed by dimuons from J/ψ decay. The J/ψ muons probe down to a P_T of 1.4 GeV/c since muons of lower P_T are stopped within the calorimeter. In Section 6, possible systematic effects at lower P_T will be studied using $\psi(2S) \to J/\psi\pi^+\pi^-$ and $B^0 \to J/\psi K^{*0}$ decays.

4.5 Momentum Scale

The overall momentum scale is set by requiring the reconstructed J/ψ mass determined by a binned-likelihood fit of Fig. 2 to be equal to the world average. After the corrections which have been discussed, we find a J/ψ mass of $3096.5^{+0.6}_{-0.9}$ MeV/c^2

which agrees well with the world average of 3096.93 MeV/c^2. Table 1 shows the contributions to the measurement uncertainty of the J/ψ mass. The J/ψ mass depends on both the momentum scale factor (equivalently the magnetic field) and the dE/dx correction. We can express the change in reconstructed J/ψ mass as a function of a small (< 0.02 kG) change in the magnetic field, B, and a small (<30%) change in the dE/dx correction, δD.

$$\Delta \mathrm{M}(J/\psi) = 0.22 \frac{\mathrm{MeV}/c^2}{\mathrm{Gauss}} \times \delta \mathrm{B} + 3.6 \mathrm{MeV}/c^2 \times \delta D \tag{4}$$

Using our best knowledge of the dE/dx correction, the momenta of tracks in this analysis are scaled by $1.00014^{+0.00030}_{-0.00020}$ to adjust the measured mass to the world average. This momentum scale factor is equivalent to using an average magnetic field (see Eq. 1) of $14.127^{+0.004}_{-0.003}$ kG compared with the measured value of 14.125 kG.

Effect	Uncertainty (MeV/c^2)
Statistical	0.1
Internal bremsstrahlung	0.2
Background shape	0.1
Subtotal fit uncertainty	0.3
dE/dx correction	$^{+0.5}_{-0.9}$
Total uncertainty	$^{+0.6}_{-0.9}$

Table 1: Summary of the contributions to the uncertainty in the J/ψ measured mass.

The momentum scale is checked by reconstructing $\Upsilon \to \mu^+\mu^-$. Figure 5 shows the reconstructed $\Upsilon \to \mu^+\mu^-$ with a binned likelihood fit to a Gaussian and second order polynomial. Including an additive correction of 3 $\pm$ 1 MeV/c^2 determined from Monte Carlo for internal bremsstrahlung, we find the mass of the $\Upsilon(1S)$ to be 9459.6 $\pm$ 2.2(stat) $^{+2.1}_{-1.8}$(syst) MeV/c^2 which agrees well with the world average mass of 9460.4 $\pm$ 0.2 MeV/c^2 [6]. The $\Upsilon(2S)$ and $\Upsilon(3S)$ states are also reconstructed at masses which agree with the world averages within our statistical precision.

5 B Meson Reconstruction

All charged tracks passing quality cuts are considered as pion and kaon candidates. These quality cuts require that the track be measured in three dimensions by the CTC and must have a minimum of 4 (2) associated hits on a minimum of 4 axial (2 stereo) superlayers. The daughter meson (K, K^{*0}, or ϕ) in $B^+ \to J/\psi K^+$, $B^0 \to J/\psi K^{*0}$, and $B_s^0 \to J/\psi\phi$ decays is selected as follows. The K is any charged track. The K^{*0} candidate consists of any two oppositely charged tracks that have an invariant mass in a $\pm$ 50 MeV/c^2 window around 896.1 MeV/c^2 when one track is assigned a kaon mass and one a pion mass. In the case where the opposite $K - \pi$ mass assignment also is consistent with being a K^{*0}, only the candidate closest to the K^{*0} mass is used. Monte

Carlo studies allow us to estimate that this procedure is correct approximately 75% of the time with insignificant loss of mass resolution. A ϕ candidate consists of any two oppositely charged tracks which have an invariant mass within 10 MeV/c^2 of the ϕ mass. The narrowness of the ϕ resonance relative to the K^{*0} reduces considerably the combinatoric background in the $B_s^0 \to J/\psi\phi$ reconstruction.

Combining all K, K^{*0}, and ϕ candidates with the J/ψ results in large combinatorial backgrounds in the B meson mass region. These backgrounds are reduced relative to the respective signals using constrained fitting techniques to improve the mass resolution. In addition, selection criteria on the transverse momentum of the daughter and B mesons and on the proper lifetime improve signal-to-noise.

5.1 Constrained Fitting

The primary collision vertex in r-ϕ is determined by using SVX track measurements averaged over many events. The uncertainty is dominated by the beam spot size of $\sim$ 40 μm. The VTX provides the z primary vertex position event-by-event with an uncertainty of 500 μm.

When the respective tracks of the daughter mesons are combined with a J/ψ candidate, a simultaneous constraint is performed where the dimuons are constrained to have the J/ψ mass, all tracks originate from a common secondary vertex, and the momentum vector of the B candidate points back along the line from the secondary vertex to the primary collision vertex in the r-ϕ plane. From the constrained fit, the secondary vertex is determined and the resolution of the track parameters are improved. For $B^+ \to J/\psi K^+$ reconstruction (see Fig. 6), the mass resolution as determined by the σ of a binned-Gaussian fit is improved from 37 to 14 MeV/c^2. In addition, a CL(χ^2) from the fit is calculated using the changes in the respective track parameters relative to measurement uncertainties. A requirement that CL(χ^2) $> 1\%$ removes combinatoric background associated with track candidates which are inconsistent with the constraint or are mismeasured.

5.2 Selection Criteria

Requirements imposed upon the transverse momenta of the daughter and of the reconstructed B mesons improve signal-to-noise of the reconstructed states. These requirements were selected on the basis of Monte Carlo studies of the kinematics of the particles involved in $B \to J/\psi X$ decays reconstructed by CDF. The selection criteria can be examined in the data using the sideband-subtracted B meson signal regions to estimate (to within approximately 10%) the observed efficiency of the different requirements. The requirement that the transverse momentum of the reconstructed B meson candidate be larger than 6 (8) GeV/c given the kaon has a P_T above 2 GeV/c is 95 (80)% efficient for signal and only 60 (30)% efficient for combinatoric background.

The B mesons under study all have a lifetime of approximately 1.5 ps [15] which can be distinguished from a zero lifetime expected for tracks originating from the primary vertex. When the reconstructed B has at least two SVX tracks (true for approximately 50% of the candidates), the $c\tau$ resolution is $\sim$ 50 μm (otherwise the

resolution is nominally ~ 200 μm). For the case where at least two of the final state tracks have SVX information, the requirement that $c\tau > 0$ (100) μm is $\sim 85(70)\%$ efficient for signal and only $\sim 55(25)\%$ efficient for the background. When the secondary vertex is not measured by the SVX, a requirement of $c\tau > 0$ (100) μm is $\sim 70(60)\%$ efficient for signal and only $\sim 55(45)\%$ efficient for background. The looser requirement that $c\tau$ be positive is made for B_s^0 candidates since the combinatoric background is relatively smaller due to the narrow window used to select ϕ candidates.

Table 2 summarizes the set of selection criteria which will be used for each of the reconstructed B mesons.

		Selection Quantity		Signal	Sideband
$B \to J/\psi X$	P_T(X)	P_T(B)	$c\tau$	Window	Window
Decay	(GeV/c)	(GeV/c)	(μm)	(GeV/c^2)	(GeV/c^2)
$B^+ \to J/\psi K^+$	>2	>8	>100	5.22 – 5.32	5.4 – 5.8
$B^0 \to J/\psi K^{*0}$	>3	>8	>100	5.22 – 5.32	5.4 – 5.8
$B_s^0 \to J/\psi\phi$	>2	>6	>0	5.32 – 5.42	5.5 – 5.9
K^{*0} within $\pm$ 50 MeV/c^2 of 896.1 MeV/c^2					
ϕ within $\pm$ 10 MeV/c^2 of 1019.4 MeV/c^2					

Table 2: Final selection criteria used to reconstruct B mesons.

6 Mass Determination

Figure 6 shows the reconstructed decays (a) $B^+ \to J/\psi K^+$ and (b) $B^0 \to J/\psi K^{*0}$ using the selection criteria of Tab. 2. Figure 7 similarly shows the reconstructed decay $B_s^0 \to J/\psi\phi$.

6.1 Mass Fits

The data in Figs. 6 and 7 are fit (excluding the region below M(B) - M(π)) using an unbinned likelihood fit assuming a Gaussian signal on a linear background. In the fit, the calculated mass uncertainty of a given candidate, obtained by propagating the track parameter uncertainties (already multiplied by 1.8), is scaled by an additional factor of 1.3 to obtain agreement with the observed mass resolution. We find 147 ± 14 B^+ candidates at a mass of 5279.1 ± 1.7 MeV/c^2, 51 ± 8 B^0 candidates at a mass of 5281.3 ± 2.2 MeV/c^2, and 32 ± 6 B_s^0 candidates at a mass of 5369.9 ± 2.3 MeV/c^2. Performing a binned likelihood fit to a linear background and Gaussian signal shape gives measured resolutions of 14.4 ± 1.6 MeV/c^2 for B^+, 11.5 ± 1.9 MeV/c^2 for B^0, and 10.4 ± 2.6 MeV/c^2 for B_s^0.

6.2 Systematic Uncertainties

Systematic uncertainties on the mass measurement arise from several sources. Each effect has been studied with signal and sideband events of all three reconstructed B mesons. To the precision that the systematic uncertainty is quoted, the effect is the same for all three states unless otherwise noted.

6.2.1 Measurement Uncertainties of the Track Parameters

The covariance matrix which describes uncertainties of the individual fitted track parameters is corrected by a multiplication factor of 1.8. This scale factor has been varied in magnitude and varied asymmetrically between the transverse and longitudinal track parameters. In these studies, no systematic shift in B meson masses are seen. The fit procedure uses individual event mass uncertainties and is thus sensitive to our uncertainty in the covariance matrix. Variations in the fitted mass were seen if the mass uncertainty scale factor, nominally 1.3, was varied between bounds of 1.0 and 1.5 where the mass uncertainty is under and over estimated. The maximum effect over all three resonances was 0.3 MeV/c^2 which is taken as a common systematic due to our incomplete understanding of the uncertainties on measured track parameters.

6.2.2 Selection Criteria

Each of the selection criteria for each of the states is varied to study possible systematic effects. Over a large range of P_T cuts, $c\tau$ and CL(χ^2) requirements, and the mass windows used to define the daughter mesons, no statistically significant systematic effects are observed.

6.2.3 $\Delta \cot\theta$

The effect of scaling $\cot\theta$ by 0.9985 ± 0.0008 is studied by applying the extreme range of the $\cot\theta$ scale to tracks of B candidates and sideband events. The mean of the event-by-event mass differences for the B^+, B^0, and B_s^0 mesons allows the assignment of systematic uncertainties of 0.8 MeV/c^2, 0.9 MeV/c^2, and 0.6 MeV/c^2 respectively.

6.2.4 Momentum Scale and Energy Loss

The event-by-event mass differences for B candidates and the sideband events are studied when the momentum scale factor (expressed in terms of the magnetic field) and the size of the dE/dx correction are varied. All three B states behave similarly upon small variations in the magnetic field and dE/dx correction represented by the following:

$$\Delta \mathrm{M}(B) = 0.11 \frac{\mathrm{MeV}/c^2}{\mathrm{Gauss}} \times \delta \mathrm{B} + 2.6 \mathrm{MeV}/c^2 \times \delta D \qquad (5)$$

The momentum scale factor and the dE/dx correction have been varied within their uncertainties while requiring that the resultant change in J/ψ mass given by Eq. 4 remain stable to within the 0.3 MeV/c^2 mass fit uncertainty. Each of the B candidates shifts maximally by 0.4 MeV/c^2 which is taken as the systematic uncertainty.

6.2.5 Checks at Low P_T

The P_T distribution of K candidates from ϕ decay for the B_s^0 candidates begins at $\sim$ 0.7 GeV/c. Since muons in $J/\psi \to \mu^+\mu^-$ decays have P_T above 1.4 GeV/c we make further checks to insure that there is no systematic effect present at lower transverse momentum. We check for this effect using two samples. The decay $\psi(2S) \to J/\psi\pi^+\pi^-$ is reconstructed with $P_T(\pi)$ beginning at 0.4 GeV/c where our track reconstruction begins to become efficient. Fig. 8 shows the reconstruction of $\psi(2S)$ using a vertex constraint and dimuon mass constraint when requiring the dipion mass to be between 0.45 and 0.58 GeV/c^2 and CL(χ^2) $> 1\%$. The fitted mass value of 3685.9 $\pm$ 0.2 MeV/c^2 agrees with the world average of 3686.00 $\pm$ 0.09 MeV/c^2 [6]. We also note that either the K or π in K^{*0} decays for B^0 candidates have P_T below 2.0 GeV/c approximately 50% of the time. Since the reconstructed B^0 mass is also in agreement with its world average, we assign no additional systematic uncertainty on the momentum scale at low P_T.

6.2.6 Other Systematics Effects

Using the large statistics sample of $J/\psi \to \mu^+\mu^-$ decays, systematic effects such as the precision to which the momentum scale is known on average can be quantified. In addition, residual systematic effects such as the dependence on $\Delta\cot\theta$ have been corrected. The resulting systematic effects on B_s^0 mass determination from these sources is small (0.7 MeV/c^2). However, there are non-Gaussian tails in many of the tracking distributions. We can estimate the contribution of remaining possible systematics from the fact that the mass difference between B^+ and B^0 has been measured to be 0.34 $\pm$ 0.29 MeV/c^2 [6]). We measure a consistent mass difference of 2.2 $\pm$ 2.8 MeV/c^2. The 2.8 MeV/c^2 statistical uncertainty provides an estimate of an upper bound for other unaccounted systematic effects. To improve the statistical power of our estimate of other systematic effects, we consider B sideband track combinations which are kinematically consistent with coming from one of the three decays and which are consistent with coming from the primary vertex. By comparing the constrained fit and unconstrained fit masses for these events (*i.e.* how much the constrained fit moves the mass is a measure of how much a systematic could affect the mass), we find the statistical precision to which we see no systematic shift to be approximately 1 MeV/c^2. We assign this 1 MeV/c^2 systematic to account for possible mass shifts due to effects which are not yet understood.

7 Conclusion

The following decays have been fully reconstructed: $B^+ \to J/\psi K^+$, $B^0 \to J/\psi K^{*0}$, and $B_s^0 \to J/\psi\phi$. In each case, the $J/\psi \to \mu^+\mu^-$ decay is used to allow the event to be recorded for analysis. The mass of each state is determined using an unbinned likelihood fit. Several sources of systematic uncertainty are summarized in Tab. 3. The measured masses of the B^+, B^0, and B_s^0 mesons are shown in Tab. 7.

Systematic Effect	B^+ Uncertainty (MeV/c^2)	B^0 Uncertainty (MeV/c^2)	B_s^0 Uncertainty (MeV/c^2)
Covariance Matrix	0.3	0.3	0.3
$\Delta\cot\theta$ Effect	0.8	0.9	0.6
Momentum Scale	0.4	0.4	0.4
Other Effects	1.0	1.0	1.0
Total (MeV/c^2)	1.4	1.4	1.3

Table 3: Contributions to the systematic uncertainties in the B meson measured masses.

B Meson	Measured Mass (MeV/c^2)	Statistical Uncertainty (MeV/c^2)	Systematic Uncertainty (MeV/c^2)
B^+	5279.1	1.7	1.4
B^0	5281.3	2.2	1.4
B_s^0	5369.9	2.3	1.3

Table 4: Summary of the measured B meson masses.

The difference between this result and our previously published value of the B_s^0 mass ($5383.3 \pm 4.5 \pm 5.0$ MeV/c^2) [8] has been studied in detail and results primarily from statistical fluctuations. The individual masses of B_s^0 candidates (signal and sideband) common to the previous analysis and the current analysis show a systematic difference of 3.0 ± 0.5 MeV/c^2. New signal events at lower measured masses and four previous signal events within 1 MeV/c^2 of a histogram bin edge (a binned fit was used in the previous analysis) account for most of the difference with our previous value.

Taking the systematic uncertainties associated with the momentum scale and $\Delta\cot\theta$ as common systematics, we calculate the mass difference between M(B_s^0) and M(B), defined as the average of the measured B^+ and B^0 states. We derive a mass difference of $89.7\pm2.7\pm1.2$ MeV/c^2. Both the measured B_s^0 mass and the mass difference are in agreement with theoretical predictions.

8 Acknowledgements

We thank the Fermilab staff and the technical staffs of the participating institutions for their vital contributions. This work was supported by the U.S. Department of Energy and National Science Foundation; the Italian Istituto Nazionale di Fisica Nucleare; the Ministry of Education, Science and Culture of Japan; the Natural Sciences and Engineering Research Council of Canada; the National Science Council of the Republic of China; and the A. P. Sloan Foundation.

References

[1] References to a specific charge state also pertain to the charge conjugate state.

[2] M. Mangano and P. Nason. Nucl. Phys. B373, 295 (1992).

[3] CDF Collaboration, F. Abe *et al.*, Phys. Rev. Lett. 75, 1451 (1995).

[4] W. Kwong and J. Rosner, Phys. Rev. D**44**, 212 (1991).

[5] A. Duncan *et al.*, Phys. Rev. D**51**, 5101 (1995).

[6] Particle Data Group, Phys. Rev. D **50** (1994).

[7] DELPHI Collaboration, P. Abreau *et al.*, Phys. Lett. **B324**, 500 (1994); ALEPH Collaboration, D. Buskulic *et al.*, Phys. Lett. **B316**, 631 (1993) and Phys. Lett. **B311**, 425 (1993); OPAL Collaboration, P. T. Acton *et al.*, Phys. Lett **B295**, 357 (1992).

[8] CDF Collaboration, F. Abe *et al.*, Phys. Rev. Lett. 71, 1685 (1993).

[9] CDF Collaboration, F. Abe *et al.*, Nucl. Instrum. Methods Phys. Res., Sect. A **271**, 387 (1988); F. Bedeschi *et al.*, Nucl. Instrum. Methods Phys. Res., Sect. A **268**, 50 (1988); G. Ascoli *et al.*, Nucl. Instrum. Methods Phys. Res., Sect. A **268**, 33 (1988).

[10] CDF Collaboration, F. Abe *et al.*, Phys. Rev. **D50**, 2966 (1994).

[11] D. Amidei *et al.*, Nucl. Instrum. Methods Phys. Res. , Sect. A **350**, 73 (1994).

[12] In CDF, ϕ is the azimuthal angle, θ is the polar angle and r is the radius from the proton beam axis (z axis).

[13] C. Newman-Holmes, E. E. Schmidt, and R. Yamada, Nucl. Instrum. Methods Phys. Res. , Sect. A **274**, 443 (1989).

[14] F. Abe *et al.*, FERMILAB-PUB-95/003-E, submitted to Phys. Rev. **D**, (1995).

[15] F. Abe *et al.*, Phys. Rev. Lett. **74**, 4988 (1995); F. Abe *et al.*, Phys. Rev. Lett. **72**, 3456 (1994).

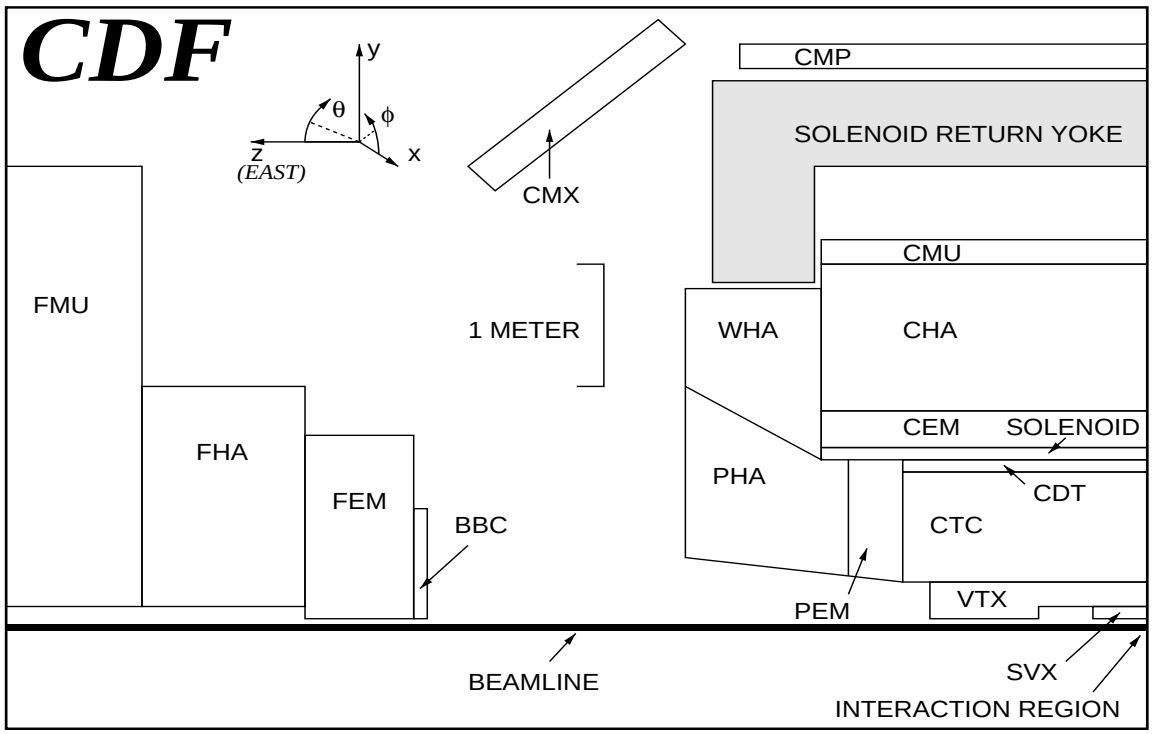

Figure 1: Side view representation of the CDF detector used in the 1992–1993 run.

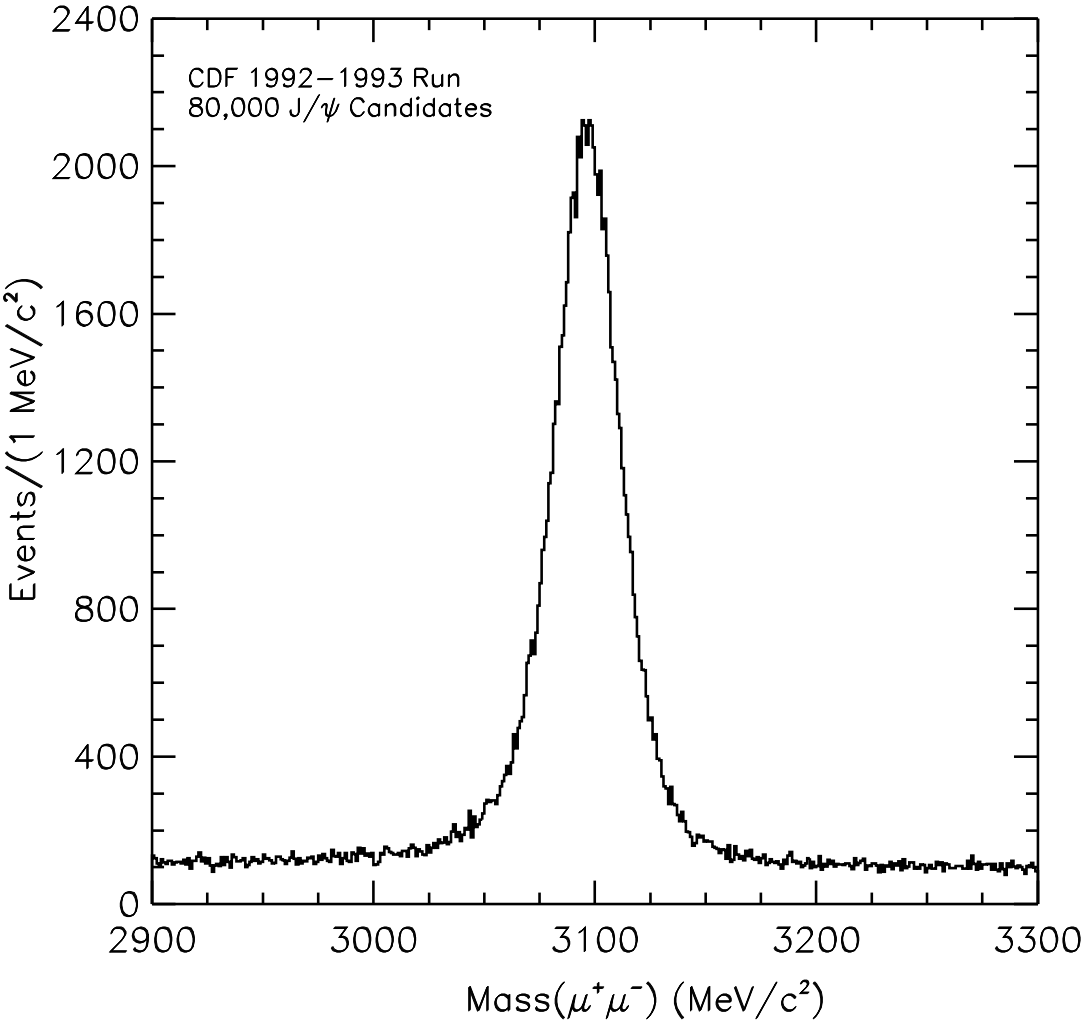

Figure 2: Dimuon mass distribution from the CDF 1992–1993 run.

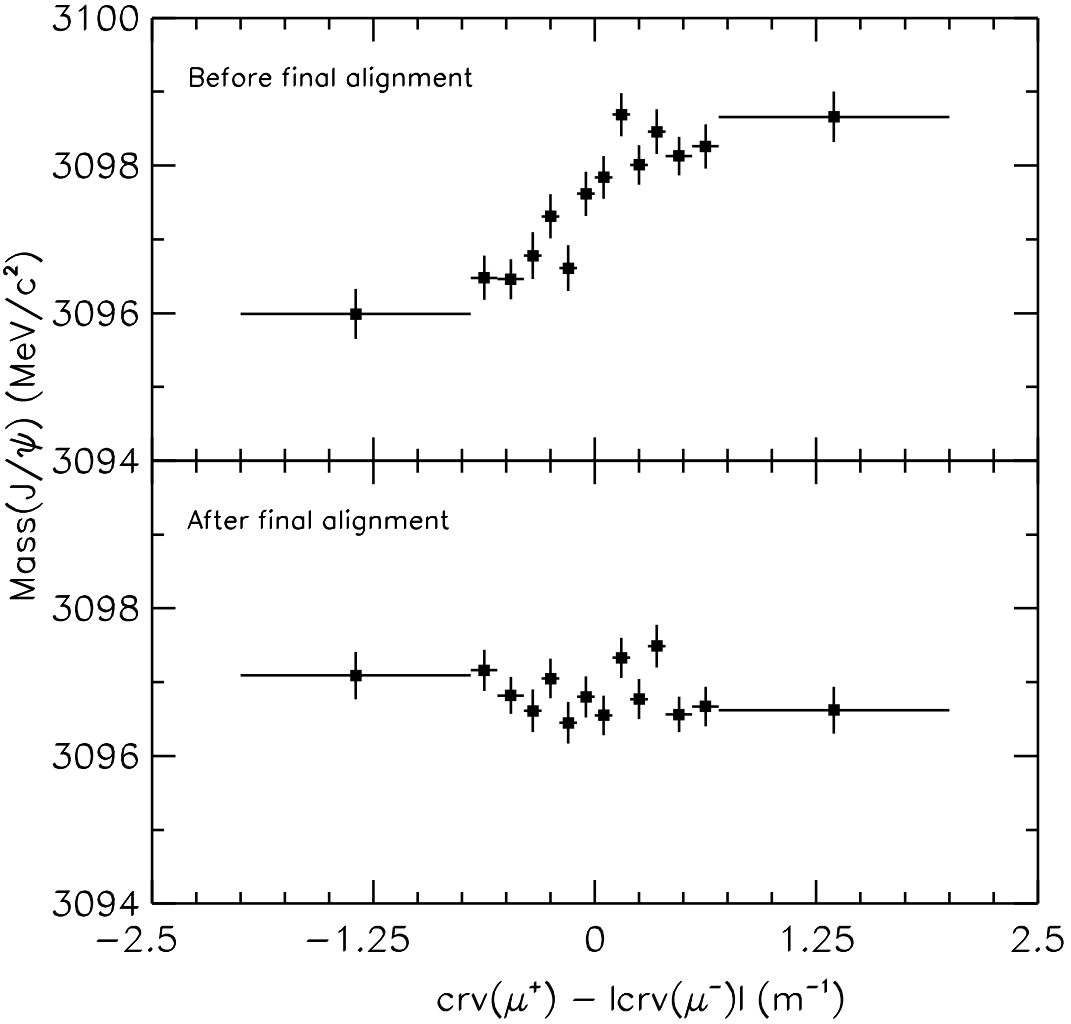

Figure 3: False curvature tracking systematic effect observed when the J/ψ mass is plotted versus the difference in absolute curvature for the positive and negative muons. The effect is removed upon applying alignment corrections as used for the tracks in this analysis.

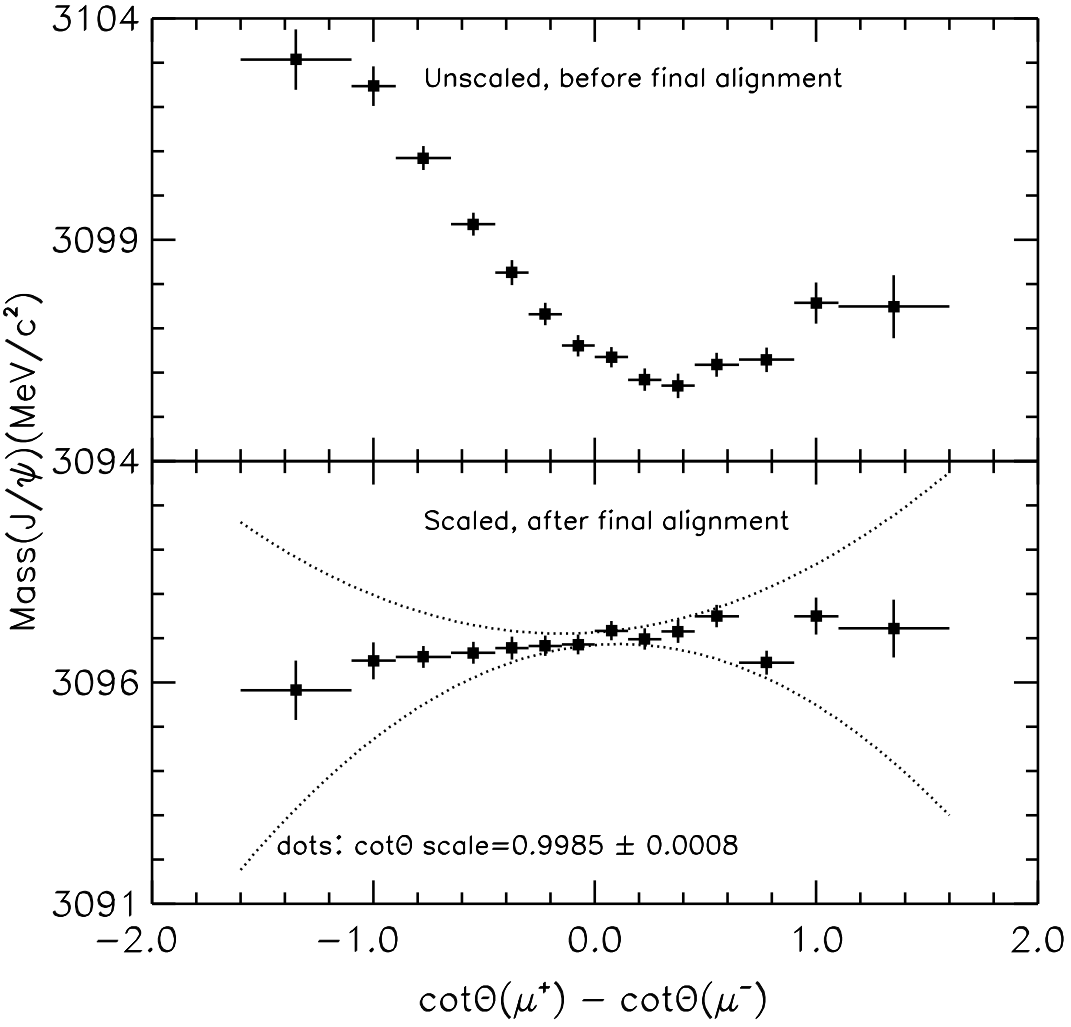

Figure 4: A systematic effect observed when the J/ψ mass is plotted versus the difference in the $\cot\theta$ between the two muons. The effect is mitigated after final CTC alignment and after scaling $\cot\theta$ by 0.9985 ± 0.008. The dotted lines show the effect at the extreme bounds of the scale factor used for determining systematic uncertainties.

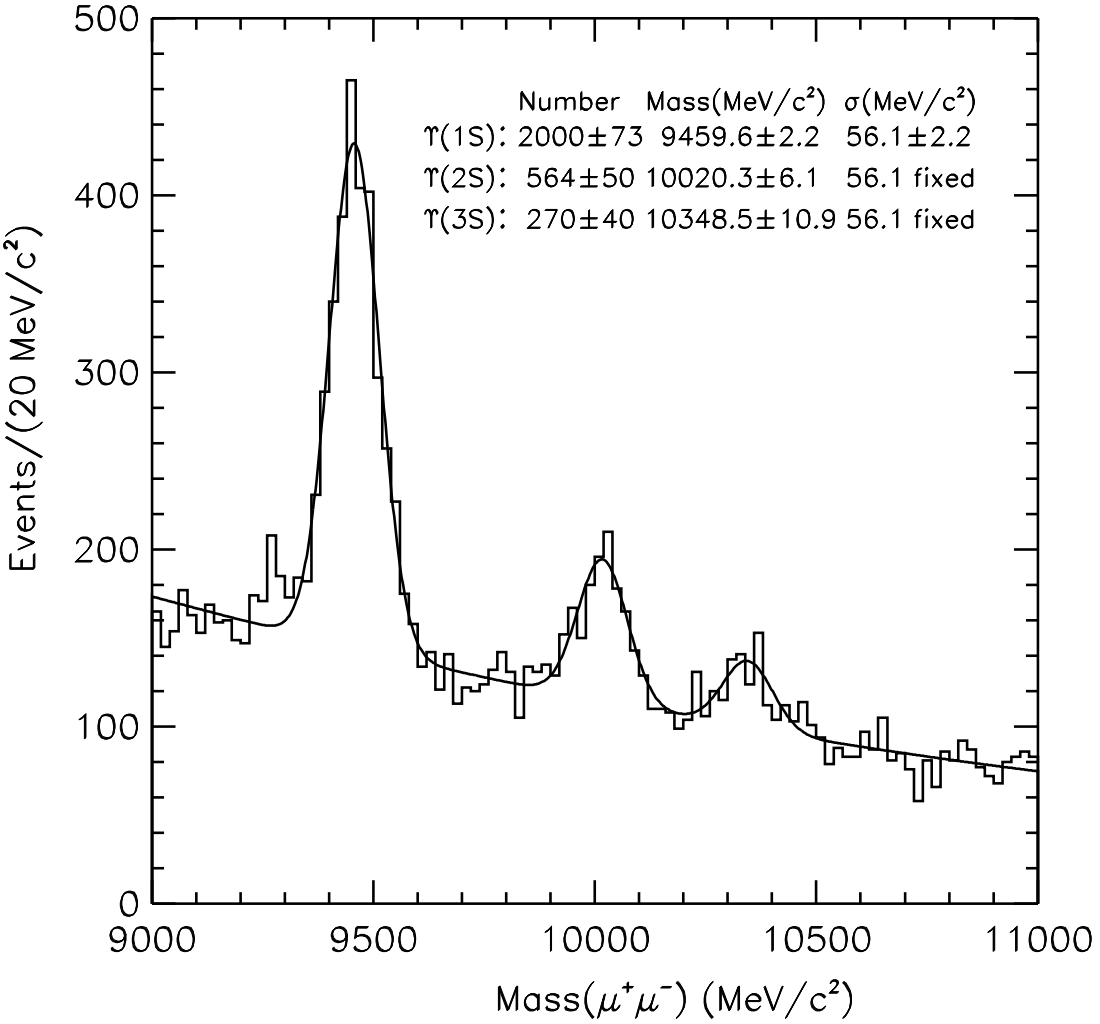

Figure 5: Reconstruction of $\Upsilon \to \mu^+\mu^-$ after applying all corrections and scale factors used to set the $J/\psi \to \mu^+\mu^-$ peak at the J/ψ mass. All Υ states agree within the statistical uncertainty to the world average masses.

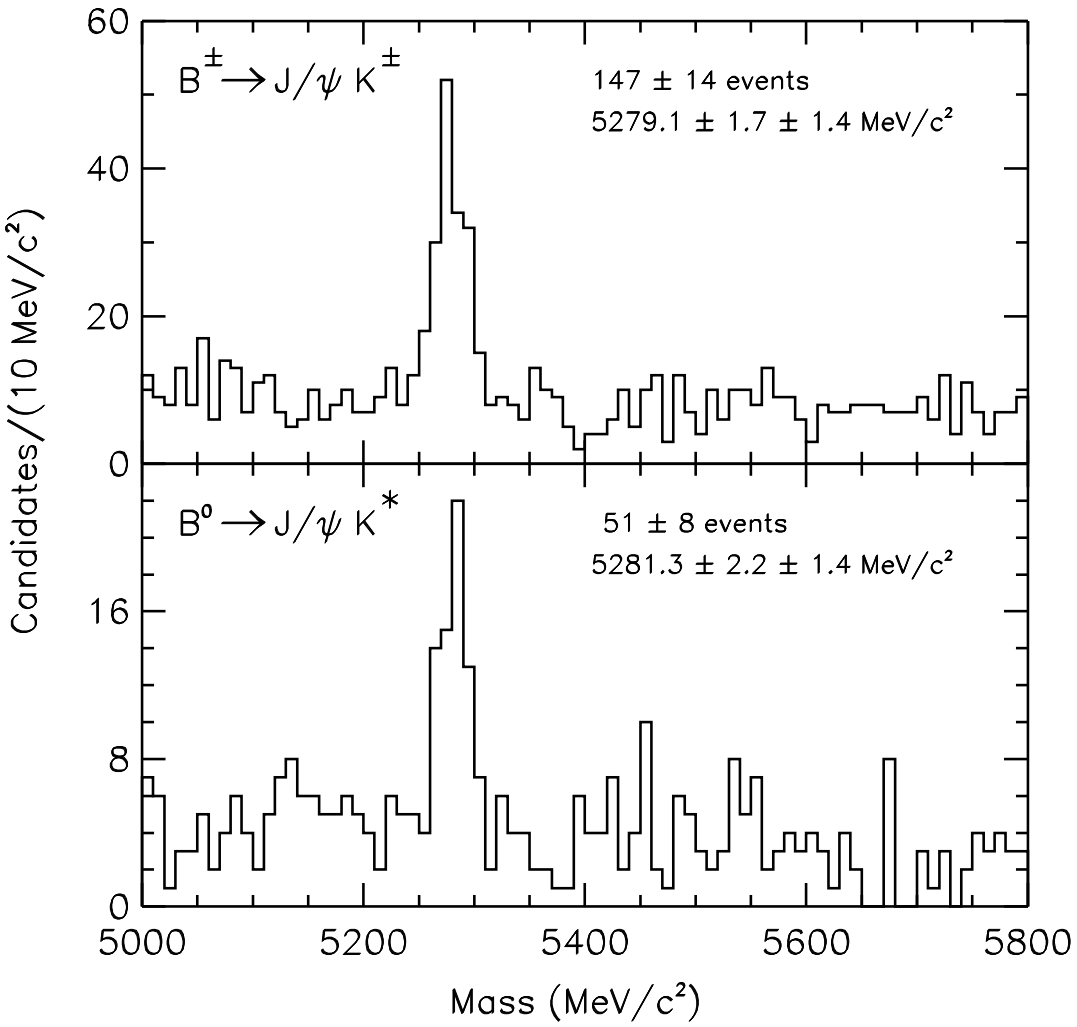

Figure 6: (a) $J/\psi K^+$ mass distribution and (b) $J/\psi K^{*0}$ mass distributions for the events passing the B^+ and B^0 selection criteria. The mass is determined by an unbinned likelihood fit of a Gaussian signal and a linear background. The quoted systematic uncertainty is evaluated within the text.

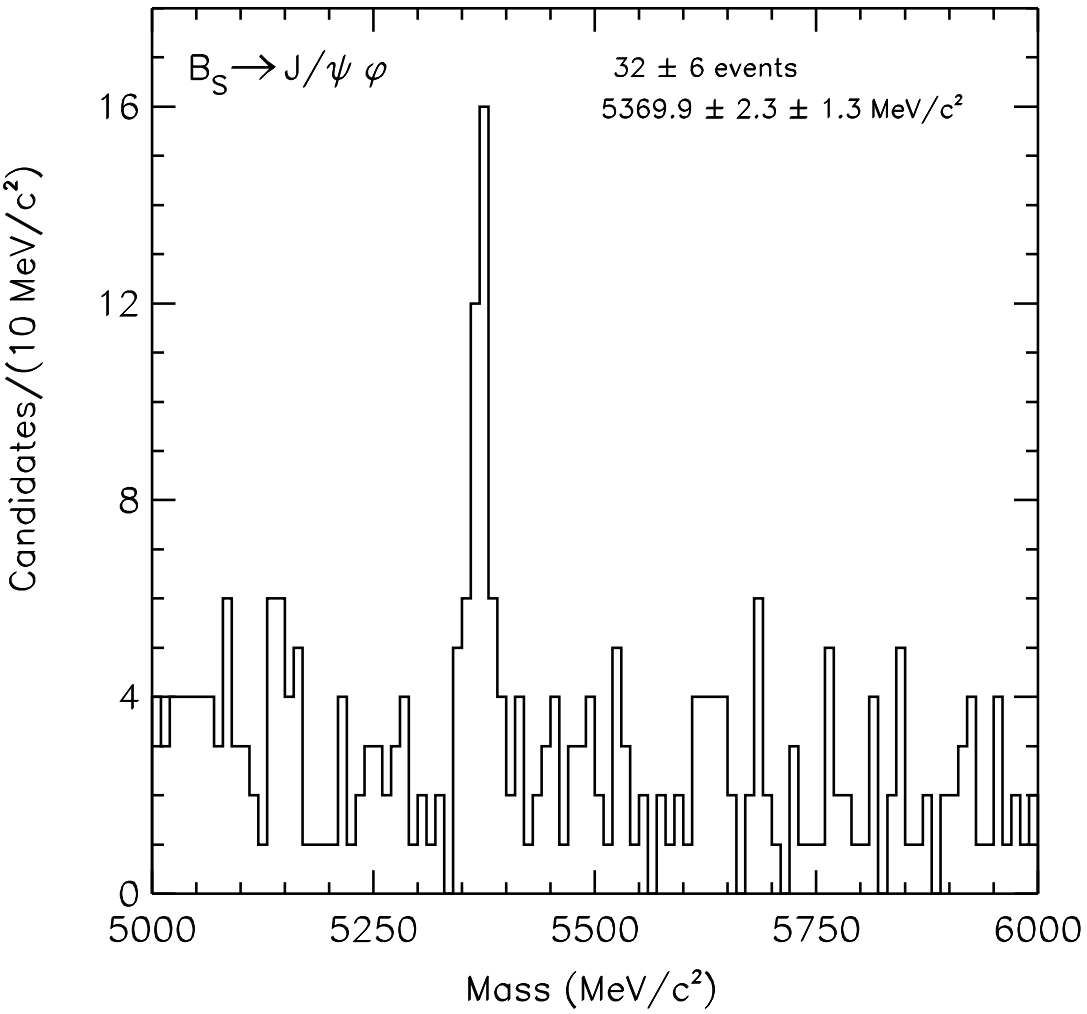

Figure 7: $J/\psi K^+K^-$ mass distribution for the events passing the B_s^0 selection criteria. The mass is determined by an unbinned likelihood fit of a Gaussian signal and a linear background. The quoted systematic uncertainty is evaluated within the text.

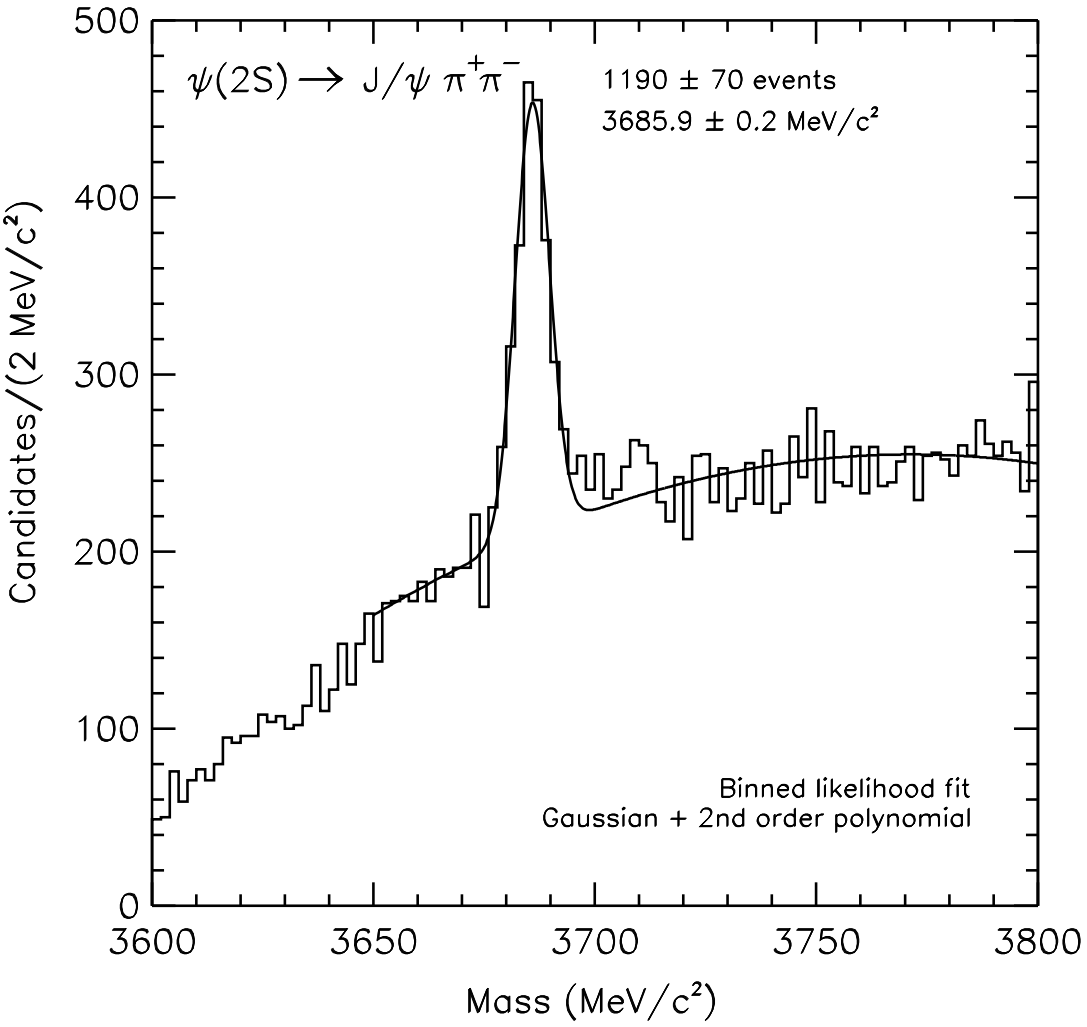

Figure 8: Mass distribution for the reconstruction of $\psi(2S) \rightarrow J/\psi\pi^+\pi^-$.